Itinerant versus localized magnetism in spin-gapped metallic half-Heusler compounds: Stoner criterion and magnetic interactions

E. Şaşıoğlu, 1,* W. Beida, 2,3 S. Ghosh, 4 M. Tas, 5 B. Sanyal, 6 S. Lounis, 1 S. Blügel, 3 I. Mertig, 1 and I. Galanakis, 7,†

1 Institute of Physics, Martin Luther University Halle-Wittenberg, 06120 Halle (Saale), Germany

2 Physics Department, RWTH Aachen University, 52062 Aachen, Germany

3 Peter Grünberg Institut, Forschungszentrum Jülich and JARA, 52425 Jülich, Germany

4 Department of Physics, Central University of Kashmir, Tulmulla, Ganderbal, Jammu and Kashmir 191131, India

5 Department of Physics, Gebze Technical University, 41400 Kocaeli, Turkey

6 Department of Physics and Astronomy, Uppsala University, 75120 Uppsala, Sweden

7 Department of Materials Science, School of Natural Sciences, University of Patras, GR-26504 Patras, Greece

(Received 6 May 2025; revised 23 September 2025; accepted 27 October 2025; published 14 November 2025)

Spin-gapped metals have recently emerged as promising candidates for spintronic and nanoelectronic applications, enabling functionalities such as sub-60 mV/dec switching, negative differential resistance, and nonlocal spin-valve effects in field-effect transistors. Realizing these functionalities, however, requires a deeper understanding of their magnetic behavior, which is governed by a subtle interplay between localized and itinerant magnetism. This interplay is particularly complex in spin-gapped metallic half-Heusler compounds, whose magnetic properties remain largely unexplored despite previous studies of their electronic structure. In this work, we systematically investigate the magnetic behavior of spin-gapped metallic half-Heusler compounds XYZ (X = Fe, Co, Ni, Rh, Ir, Pd, Pt; Y = Ti, V, Zr, Hf, Nb, Ta; Z = In, Sn, Sb), revealing clear trends. Coand Ni-based compounds predominantly exhibit itinerant magnetism, whereas Ti-, V-, and Fe-based systems may host localized moments, itinerant moments, or a coexistence of both. To uncover the origin of magnetism, we apply the Stoner model, with the Stoner parameter I estimated from Coulomb interaction parameters (Hubbard U and Hund's exchange J) computed using the constrained random phase approximation (cRPA). Our analysis shows that compounds not satisfying the Stoner criterion tend to remain nonmagnetic. On the contrary, compounds that satisfy the Stoner criterion, generally exhibit magnetic ordering. highlighting the crucial role of electronic correlations and band structure effects in the emergence of magnetism. For compounds with magnetic ground states, we compute Heisenberg exchange parameters, estimate Curie temperatures (T_C) , and analyze spin-wave properties, including magnon dispersions and stiffness constants. These results provide microscopic insight into the magnetism of spin-gapped metallic half-Heuslers and establish a predictive framework for designing spintronic materials with tailored magnetic properties.

DOI: 10.1103/f4wj-12gt

I. INTRODUCTION

Heusler compounds constitute a remarkably versatile class of materials that exhibit a broad spectrum of exotic electronic and magnetic properties, positioning them as a central platform in the design of functional quantum materials. Originally discovered several decades ago, these intermetallics have recently attracted renewed interest because of their potential in spintronics, magnetoelectronics, and energy-related applications [1–3]. Their diverse functionalities arise from intricate interactions among the valence *d* orbitals of transition metal atoms, which can be finely tuned through compositional and structural modifications [4–9]. Among the most celebrated electronic properties of Heusler compounds is half-metallicity, in which one spin channel is metallic while the

other is insulating, resulting in 100% spin polarization at the Fermi level—an ideal characteristic for spintronic devices. A related and equally intriguing electronic structure is that of a spin gapless semiconductor, defined by a zero gap in one spin channel and a finite gap in the other, enabling high carrier mobility and efficient spin transport [4,10]. Certain Heusler compounds also exhibit magnetic semiconducting behavior, characterized by a semiconducting electronic structure combined with long-range magnetic order, which is particularly promising for spin-filtering and magneto-optical applications [11,12]. More recently, a number of Heusler compounds have been shown to host topological properties, including nontrivial surface states and Weyl nodes, driven by band inversions and symmetry-protected degeneracies [13–17]. These features position Heusler compounds at the forefront of research into quantum materials with multifunctional properties.

Among the broad family of Heusler compounds, a particularly interesting subset is formed by the 18-valence-electron half-Heusler (or semi-Heusler) systems, which are best

^{*}Contact author: ersoy.sasioglu@physik.uni-halle.de

[†]Contact author: galanakis@upatras.gr

known for their semiconducting behavior and exceptional thermoelectric performance at elevated temperatures. These materials, including well-studied examples such as CoTiSb, FeVSb, and NiTiSn, have long served as model systems for exploring structure-property relationships in Heusler compounds [7,18–25]. More recently, Şaşıoğlu and collaborators identified that certain half-Heusler compounds with one or two valence electrons more or less than these semiconductors are in fact nonmagnetic gapped metals, characterized by an energy gap just below or above the Fermi level [26]. Since the Fermi level intersects either the valence or conduction band, these gapped metals behave similarly to conventional doped semiconductors, where transport is dominated by holes or electrons, respectively. Remarkably, as shown in Ref. [26], many of the studied compounds fall into a new class of materials termed spin-gapped metals. These spin-gapped metallic Heusler compounds typically possess 16, 17, 19, or 20 valence electrons per formula unit and feature a spin-dependent energy gap near the Fermi level. Depending on the alignment of the Fermi level relative to the spin-resolved energy gaps, each spin channel can exhibit an intrinsic p- or ntype character, analogous to doped magnetic semiconductors [27–30]. This intrinsic carrier-type asymmetry in spin channels makes spin-gapped metals particularly promising for spintronic applications, as they eliminate the need for extrinsic doping and avoid associated issues such as disorder and phase separation. Moreover, recent theoretical proposals demonstrate that spin-gapped metals can serve as efficient electrode materials in multifunctional field-effect transistors, enabling device functionalities such as sub-60 mV/dec switching, negative differential resistance, and nonlocal giant magnetoresistance [31]. These features make spin-gapped metals attractive candidates for future low-power, logic-in-memory, and multivalued logic devices beyond the limits of conventional CMOS technology.

Despite their promising potential, the underlying magnetic behavior of spin-gapped metals remains poorly understood. Although Ref. [26] introduced the concept of spin-gapped metals using half-Heusler compounds as prototype materials through ab initio density functional theory calculations, several aspects of their behavior remain unexplored. For example, some Co- and Ni-based compounds unexpectedly adopt nonmagnetic ground states and behave as ordinary gapped metals, whereas others display magnetic ordering [26]. These observations raise key questions about the mechanisms that govern magnetism in these materials: Are their properties driven by conventional exchange interactions, or do they stem from more subtle electronic instabilities? Addressing these questions is essential for understanding the microscopic origin of magnetism in spin-gapped metals and for advancing their use in spintronic applications.

In this work, we address these questions by conducting a systematic investigation of half-Heusler compounds including a wide range of transition metals, including Ti, V, Fe, Co, Ni, Rh, Ir, Pd, and Pt most of which were initially identified as spin-gapped metals in Ref. [26]. By analyzing their magnetic moments, exchange interactions, and electronic structures, we uncover distinct trends in their magnetic behavior. Our results show that Co- and Ni-based compounds predominantly exhibit itinerant magnetism, whereas Ti-, V-, and Fe-based

systems can display localized or itinerant moments, or a coexistence of both. To understand the origin of this diversity, we employ a combination of density functional theory (DFT), constrained random phase approximation (cRPA), and Stoner model. This integrated approach enables us to quantify electronic correlations, evaluate magnetic instabilities, and establish a predictive framework for magnetism in spin-gapped metallic half-Heusler compounds. Our findings not only provide microscopic insights into the mechanisms governing magnetism in these systems but also lay the groundwork for designing spintronic materials with tailored magnetic properties.

The remainder of this paper is organized as follows. In Sec. II, we provide an overview of the materials studied in this work, based primarily on the spin-gapped metallic half-Heusler compounds identified in Ref. [26]. Section III describes the first-principles electronic structure methods employed, along with the theoretical models and approximations used to analyze magnetism and electronic correlations. In Sec. IV, we present and discuss our results in detail. Section IV A focuses on the nature of magnetism in each compound, identifying whether the moments are itinerant, localized, or coexisting. In Sec. IVB, we briefly discuss the on-site effective Coulomb interaction parameters, which are subsequently used in Sec. IV C to compute the Stoner parameter and evaluate the tendency of the paramagnetic state toward ferromagnetic instability. Section IVD analyzes the stability of the magnetic ground state through calculated exchange constants, and further estimates Curie temperatures and spinwave properties. Finally, Sec. V summarizes the main findings and outlines the broader implications of our work.

II. SPIN-GAPPED METALS

To lay the groundwork for understanding the magnetic behavior of spin-gapped half-Heusler compounds, we begin by examining their characteristic electronic structure features. Figure 1 schematically illustrates the density of states (DOS) for normal metals, gapped metals, and spin-gapped metals. In normal metals, the Fermi level intersects both spin channels of the band structure, and no energy gap exists in its vicinity. In contrast, gapped metals exhibit a gap near the Fermi level. Unlike semiconductors, where the Fermi level lies within the gap, in gapped metals the Fermi level either intersects the valence band—resulting in p-type behavior, or the conduction band, yielding n-type behavior as shown in Figs. 1(b) and 1(c). In the p-type case, holes are available for transport, while in the *n*-type case, electrons are available, analogous to doped semiconductors. In spin-gapped metals, the DOS becomes spin-dependent because of magnetic ordering, and the two spin channels exhibit distinct energy gaps. The position of these gaps relative to the Fermi level determines the carrier type for each spin channel. Depending on this alignment, both spin channels can display p-type or *n*-type behavior [Figs. 1(d) and 1(e)], or a mixed case can arise [Fig. 1(f)], in which one spin channel is p type while the other is n type. To characterize these systems in more detail, we define four key electronic structure parameters, as depicted in Fig. 1: the internal band gap $(E_{\mathfrak{g}}^{\mathrm{I}})$, the external band gap $(E_{\mathfrak{g}}^{\mathrm{E}})$, and the internal and external metallic bandwidths,

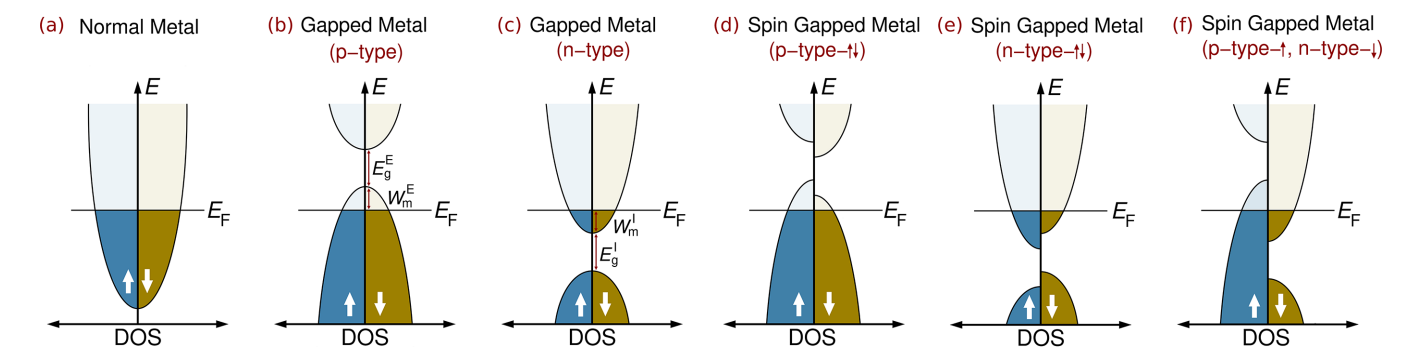


FIG. 1. Schematic representation of the density of states (DOS) of a normal metal (a), gapped metals (b)(c), and spin-gapped metals (d)–(f). The arrows represent the two possible spin directions. The horizontal line depicts the Fermi level E_F .

 $W_{\mathrm{m}}^{\mathrm{I}}$ and $W_{\mathrm{m}}^{\mathrm{E}}$, respectively. $W_{\mathrm{m}}^{\mathrm{E}}$ denotes the energy difference between the Fermi level and the valence band maximum for p-type gapped or spin-gapped metals, while $W_{\mathrm{m}}^{\mathrm{I}}$ is the energy difference between the conduction band minimum and the Fermi level in n-type systems.

Based on the electronic classification outlined above, we now turn to the specific set of spin-gapped half-Heusler compounds investigated in this study. In Ref. [26], we identified spin-gapped metals among half-Heusler compounds with 16, 17, and 19 valence electrons by performing a highthroughput screening using the Open Quantum Materials Database (OQMD) [32-34]. The selection criteria for candidate compounds were twofold. First, the formation energy E_{form} had to be negative to ensure thermodynamic stability. Second, the convex hull distance ΔE_{con} —the energy difference between the considered structure and the most stable phase or mixture of phases—was required to be less than 0.2 eV/atom, a threshold that supports the experimental feasibility of synthesizing metastable compounds. Table I summarizes all spin-gapped metals studied in Ref. [26], excluding CuVSb because of its relatively large convex hull distance. In this work, we expand that dataset by including five additional spin-gapped half-Heusler compounds: FeZrSn, FeHfSn, NiTiIn, PdTiIn, and IrVSb. In total, we investigate twenty four compounds, and their corresponding lattice constants, obtained from OQMD, are listed in Table I.

Beyond structural stability, previous studies have also revealed systematic trends in the electronic properties of these compounds, which provide important context for the magnetic behavior analyzed in this work. In Ref. [26], a detailed analysis of the spin-resolved electronic band structures was provided for each compound. For reasons of completeness, we have included in Table I the spin-gap type of the band structure for both spin channels for the compounds under study. A clear trend was identified: Compounds with fewer than 18 valence electrons generally exhibit p-type spin-gapped behavior, whereas those with more than 18 valence electrons tend to be *n*-type spin-gapped metals. The nature of spin polarization at the Fermi level further distinguishes the electronic character. The spin polarization (SP) is defined as the difference between the spin-up and spin-down DOS at the Fermi level, divided by the total DOS. If the SP is 100%, one spin channel (typically spin-down) exhibits a semiconducting character. When SP is less than 100%, both spin channels contribute to conduction and display either p- or n-type metallic behavior. Table I also lists the SP values for all compounds considered in this study. Most compounds with 16 or 17 valence electrons exhibit *p*-type spin-gapped character in both spin channels. In contrast, among the 19- or 20-valence-electron systems, only PdTiSb and PtTiSb are *n* type in both spin channels; the remaining compounds show *n*-type behavior in one spin direction, while the other exhibits semiconducting characteristics.

To complement the electronic structure perspective, it is also important to consider the crystallographic framework of the spin-gapped metals studied in this work, as crystal symmetry plays a crucial role in governing magnetic interactions and possible magnetic ordering. All bulk half-Heusler compounds with the general formula XYZ crystallize in the cubic $C1_b$ structure, which belongs to the $F\overline{4}3m$ space group. A schematic representation of this lattice is shown in Fig. 2(a) for the representative case of FeTiSb. The large cubic unit cell shown contains four primitive unit cells and can be viewed as a face-centered cubic (fcc) lattice with a four-site basis. In Wyckoff coordinates, the A site at (000) is occupied by Fe atoms, the B site at $(\frac{1}{4}, \frac{1}{4}, \frac{1}{4})$ by Ti atoms, and the D site at $(\frac{3}{4}, \frac{3}{4}, \frac{3}{4})$ by Sb atoms. The C site at $(\frac{1}{2}, \frac{1}{2}, \frac{1}{2})$ remains unoccupied—a characteristic feature of the $C1_b$ structure. From a symmetry standpoint, both the Fe and the vacant C sites are located at the centers of smaller cubes, each surrounded by four Ti and four Sb atoms as nearest neighbors at the cube corners. Conversely, each Ti or Sb atom is centered within a cube defined by four Fe atoms and four vacant C sites. Figure 2(b) shows the doubled unit cell constructed along the [111] direction, which we employ for our antiferromagnetic (AFM) calculations. The specific AFM configuration and its implications for the magnetic behavior will be discussed in Sec. IV.

III. COMPUTATIONAL DETAILS

Having established the electronic and structural characteristics of spin-gapped metallic half-Heusler compounds, we now turn to the computational framework used to investigate their magnetic behavior. In this study, we employ three distinct *ab initio* electronic structure methods to investigate the ground-state properties of spin-gapped metals. The rationale for using three different methods lies in the flexibility they offer for postprocessing and analyzing different magnetic properties. Each method provides complementary capabilities, allowing us to perform an in-depth investigation of the

TABLE I. Lattice constants (a_0) , total number of valence electrons (Z_T) , spin-gap type in each spin channel (NM stands for normal-metallic behavior, SC for semiconducting behavior and the arrows depict the spin-up and spin-down electronic band structures), sublattice and total magnetic moments for both ferro-/ferrimagnetic (FM) and antiferromagnetic (AFM) configurations, spin polarization at the Fermi level (see text for definition), spin-wave stiffness constant (D), and calculated Curie temperatures (T_C) for the studied compounds. The lattice constants a_0 are taken from the Open Quantum Materials Database [32–34].

				FM (001)			AFM (111)				
Compound <i>XYZ</i>	a ₀ (Å)	Z_T	Spin-gap type	$m_X = (\mu_B)$	$m_Y = (\mu_B)$	$m_{ ext{total}} \ (\mu_B)$	$m_X = (\mu_B)$	$m_Y = (\mu_B)$	SP (%)	$\begin{array}{c} D \\ (\text{meV Å}^2) \end{array}$	<i>T</i> _C (K)
FeZrSn	6.24	16	p -type- \uparrow/p -type- \downarrow	-2.03	0.18	-1.90	-1.86	0.33	64	227	151
FeHfSn	6.19	16	p -type- \uparrow/p -type- \downarrow	-1.86	0.17	-1.74	-1.65	0.26	28	169	150
FeTiSb	5.94	17	p -type- \uparrow/p -type- \downarrow	-1.45	0.53	-0.95	-0.99	0.23	68	706	317
FeZrSb	6.15	17	p-type-↑/SC-↓	-1.34	0.34	-1.00	-1.08	0.16	100	738	274
FeHfSb	6.11	17	p-type-↑/SC-↓	-1.26	0.27	-1.00	-0.93	0.12	100	857	276
FeVSn	5.87	17	NM- \uparrow / p -type- \downarrow	-1.85	1.03	-0.88	-1.40	0.87	36	383	532
FeNbSn	6.00	17	p -type- \uparrow /SC- \downarrow	-1.38	0.40	-1.00	-1.05	0.23	100	734	266
FeTaSn	5.99	17	p -type- \uparrow /SC- \downarrow	-1.29	0.32	-1.00	-0.88	0.18	100	810	282
CoTiSn	5.93	17	p -type- \uparrow/p -type- \downarrow	-0.42	-0.45	-0.94	0.00	0.00	74	669	56
CoZrSn	6.15	17	p -type- \uparrow/p -type- \downarrow	-0.67	-0.18	-0.95	-0.27	0.01	81	936	126
CoHfSn	6.11	17	p -type- \uparrow/p -type- \downarrow	-0.55	-0.15	-0.79	0.00	0.00	66	897	108
RhTiSn	6.17	17	p -type- \uparrow/p -type- \downarrow	-0.07	-0.73	-0.87	0.00	0.00	70	226	131
IrTiSn	6.20	17	p -type- \uparrow/p -type- \downarrow	-0.08	-0.61	-0.76	0.00	0.00	33	165	95
NiTiIn	5.99	17	p -type- \uparrow/p -type- \downarrow	-0.04	-0.81	-0.97	0.00	0.00	97	533	141
NiZrIn	6.22	17	p -type- \uparrow/p -type- \downarrow	-0.11	-0.31	-0.55	0.00	0.00	53	177	23
PdTiIn	6.23	17	p -type- \uparrow /SC- \downarrow	-0.03	-0.87	-0.99	-0.01	-0.27	99	713	157
PtTiIn	6.24	17	p -type- \uparrow /SC- \downarrow	-0.04	-0.84	-1.00	0.01	-0.19	100	769	189
CoVSb	5.81	19	n-type-↑/SC-↓	-0.33	1.41	1.00	0.11	1.31	100	590	419
RhVSb	6.07	19	n-type-↑/SC-↓	-0.21	1.33	1.00	-0.08	1.64	100	484	228
IrVSb	6.07	19	n-type-↑/SC-↓	-0.21	1.26	1.00	-0.08	1.30	100	498	283
PdTiSb	6.24	19	n-type- $↑/n$ -type- $↓$	-0.04	0.98	0.89	-0.02	0.83	87	383	194
PtTiSb	6.26	19	n-type- $↑/n$ -type- $↓$	-0.05	1.05	0.99	-0.03	0.76	93	755	318
NiVSn	5.87	19	n-type-↑/SC-↓	-0.03	1.15	1.00	-0.03	1.77	100	250	109
NiVSb	5.88	20	<i>n</i> -type-↑/SC-↓	0.03	2.12	2.00	0.01	2.29	100	561	684

electronic and magnetic behavior of spin-gapped half-Heusler compounds. Our extensive cross-validation tests (not shown) confirm that all three methods yield nearly identical results for the systems under study when the Perdew–Burke–Ernzerhof (PBE) parametrization of the generalized gradient approximation (GGA) for the exchange-correlation functional [35] is used [36]. We have also performed test calculations (not shown here) on the spin-gapped metal FeTiSb and the non-magnetic gapped metal CoTaSb using the more sophisticated

r²SCAN meta-GGA functional [37]. Our test results revealed that both PBE and r²SCAN produce a physically consistent description of the electronic structure of both gapped and spingapped metals, which justify the use of the PBE functional in our study.

The first *ab initio* electronic structure method we employ is the QUANTUMATK software package [38,39]. This approach uses linear combinations of atomic orbitals (LCAO) as a basis set, combined with norm-conserving PseudoDojo

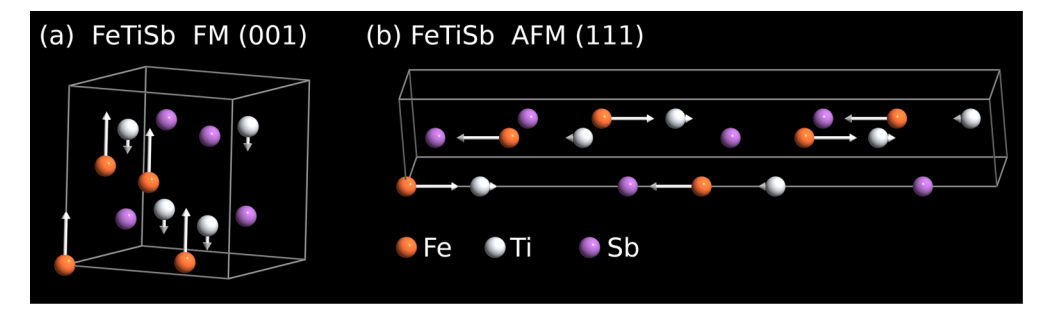


FIG. 2. Schematic representation of the unit cells used for ferro-/ferrimagnetic (FM) and antiferromagnetic (AFM) calculations, illustrated using the FeTiSb compound as an example. Panel (a) shows the conventional unit cell employed for FM calculations, where atomic spin magnetic moments (indicated by arrows) are aligned parallel to the [001] crystallographic direction. Panel (b) depicts the doubled unit cell constructed along the [111] direction for AFM calculations, in which the magnetic moments are oriented antiparallel along [111]. The length of each arrow is proportional to the magnitude of the calculated atomic spin magnetic moment.

pseudopotentials [40]. For ground-state calculations of the bulk compounds, we use a $16 \times 16 \times 16$ Monkhorst-Pack **k**-point grid [41]. In addition to ground-state calculations, the QUANTUMATK framework is used to compute magnetic interactions and excitations, making it central to our analysis of spin dynamics. Specifically, we calculate the Heisenberg exchange parameters using the Liechtenstein-Katsnelson-Antropov-Gubanov (LKAG) formalism [42], following the procedure described in Ref. [23]. These exchange constants serve as the foundation for two key analyses: estimation of Curie temperatures and evaluation of spin-wave properties. To estimate the Curie temperatures $(T_{\rm C})$, the computed exchange parameters are used within the mean-field approximation. For the spin-wave analysis, we calculate the magnon dispersions and extract spin-wave stiffness constants based on the formalism developed in Ref. [43]. This method, tailored for multisublattice magnetic systems, generalizes earlier work by Pajda et al. [44], originally formulated for singlesublattice magnets. Together, these calculations provide a comprehensive picture of the magnetic exchange interactions and excitation spectra, offering valuable insights into the potential of spin-gapped metals for high-temperature spintronic applications.

The second ab initio method employed in this work is the full-potential linearized augmented plane wave (FLAPW) approach, as implemented in the FLEUR code [45,46]. We first perform nonmagnetic ground-state calculations using FLEUR and then use the SPEX code [47,48] to compute the effective Coulomb interaction parameters within the framework of the constrained random phase approximation (cRPA). The cRPA method is a state-of-the-art approach for determining material-specific interaction parameters such as the Hubbard U and Hund's exchange J. It has been successfully applied to a variety of Heusler systems, including half-metallic [49] and Mn-based full Heusler compounds [50]. For further details on the cRPA methodology in Heusler compounds, we refer the reader to Refs. [49,50]. The obtained U and J values are then used to compute the Stoner parameter, defined as I = (U + 6J)/5 [51]. Within the Stoner model, this parameter plays a central role in predicting ferromagnetic instability through the criterion $I \times N(E_F) > 1$, where $N(E_F)$ denotes the density of states at the Fermi level.

Finally, we employ the all-electron *ab initio* full-potential nonorthogonal local-orbital minimum-basis band structure method (FPLO) [52,53]. This approach allows for an accurate and efficient treatment of the electronic structure, particularly near the atomic cores. In this work, we use the FPLO results primarily to compute and visualize the charge density isosurfaces, which will be discussed in detail in the following sections. Together, these three complementary methods enable a detailed and cross-validated analysis of the electronic, magnetic, and correlation effects in spin-gapped metallic half-Heusler compounds.

IV. RESULTS AND DISCUSSION

A. Itinerant versus localized magnetism

To gain insight into the nature of magnetism in 16-, 17-, 19-, and 20-valence-electron half-Heusler compounds,

we computed the magnetic moments for both ferromagnetic/ferrimagnetic (FM) and antiferromagnetic (AFM) configurations (Table I). For the AFM configuration, we considered a layered [111]-oriented ordering, where spin magnetic moments alternate in direction between neighboring (111) planes. This choice follows the work by Halilov et al. on elementary ferromagnets (Fe, Co, and Ni) who have shown using the spin-spiral technique that for fcc Ni the spin magnetic moment reduction, with respect to the FM configuration, is larger when one chooses the AFM[111] instead of the AFM[001] configuration [54]. The latter is favored in the case of half-Heusler compounds containing rare-earth metals like NdBiPt [55]. Test calculations on the compounds under study (not presented here) have shown that the spin-gapped metallic Heusler compounds in Table I being itinerant magnets show a preference towards the AFM[111] configuration. For the latter, the suppression of the spin magnetic moment with respect to the FM case is larger, making the AFM[111] configuration more suitable than the AFM[001] configuration in detecting the presence of itinerant magnetism. Thus in the following we present results only for this AFM configuration.

The unit cells used for FM and AFM calculations are illustrated in Fig. 2, with FeTiSb shown as a representative example. In these schematics, the arrow directions indicate spin magnetic moments orientation, while their lengths represent the magnitude of the magnetic moments. This computational setup provides a straightforward yet effective means to distinguish between localized and itinerant magnetism: in systems with localized moments, magnetic moments tend to persist even in the AFM configuration, whereas itinerant moments are typically suppressed or vanish upon switching from FM to AFM alignment. The results summarized in Table I reveal distinct trends across the different valence electron counts, highlighting a strong correlation between electronic structure and moment stability. Specifically, Fe-based 16- and 17-electron compounds exhibit relatively stable local moments in both FM and AFM states. In contrast, several 17-electron systems—particularly those based on Co, Rh, and Ni—display significant suppression or even complete collapse of the magnetic moment in the AFM configuration, consistent with itinerant behavior. Meanwhile, 19- and 20-electron compounds maintain robust magnetism with minimal variation between FM and AFM states, underscoring the role of exchange interactions in stabilizing local moments in these systems.

To understand the origin of these trends, we now examine the underlying electronic mechanisms that govern moment stability across different compound families. The collapse of magnetic moments in certain 17-valence-electron compounds can be attributed to the interplay between exchange splitting and electronic hybridization. In Co- and Rh-based systems, the relatively large *d* bandwidth leads to stronger hybridization, promoting more itinerant magnetic behavior. As a consequence, AFM ordering significantly modifies the DOS at the Fermi level, suppresses exchange splitting, and destabilizes local moments. This trend is evident in compounds such as CoTiSn and CoHfSn, where the magnetic moment completely vanishes in the AFM configuration. In contrast, Fe-based 16- and 17-electron compounds retain sizable moments even in the AFM state, indicating a more localized

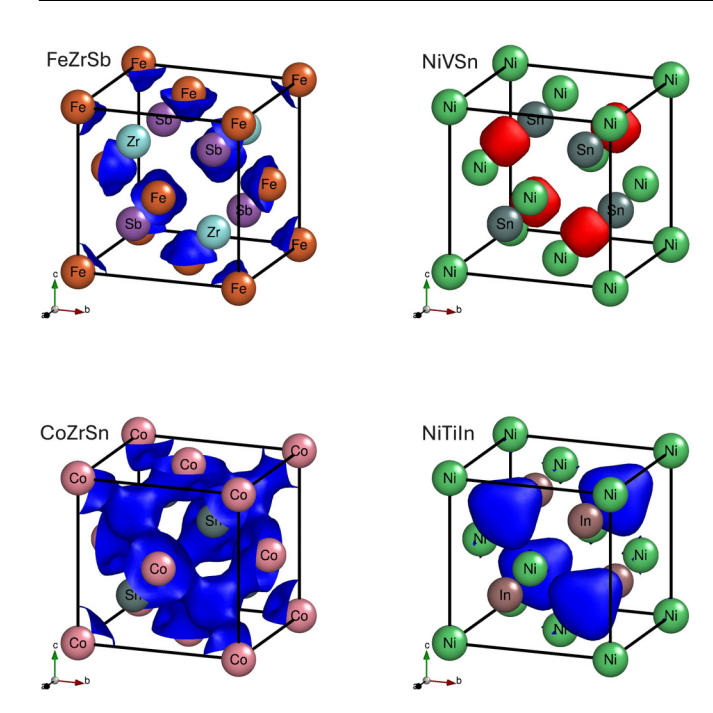


FIG. 3. Spin density isosurfaces (defined as the difference between spin-up and spin-down charge densities) for four representative compounds. FeZrSb and NiVSn exhibit localized magnetic moments centered on the Fe and V atoms, respectively. In contrast, CoZrSn and NiTiIn display itinerant magnetic behavior, with spin polarization primarily associated with the Co and Ni atoms. Positive and negative values of the spin density are represented by red and blue isosurfaces, respectively.

character of magnetism on Fe atoms, which is less sensitive to spin-ordering changes. For 19- and 20-electron compounds, such as CoVSb, RhVSb, and NiVSb, the magnetic moments in FM and AFM configurations remain largely unchanged, suggesting a robust exchange interaction that stabilizes magnetism regardless of magnetic ordering. This is particularly evident in NiVSb, where a sizable moment of approximately $2.12~\mu_B$ persists in the AFM state.

To further support these interpretations, we analyze the real-space spin density distributions, which offer direct insight into the degree of magnetic moment localization. Figure 3 presents the spin density—defined as the difference between spin-up and spin-down charge densities-for four representative compounds: FeZrSb, CoZrSn, NiVSn, and NiTiSn. In FeZrSb, which exhibits localized magnetism, the spin density is primarily concentrated around the Fe atoms. In contrast, CoZrSn displays itinerant magnetic behavior, with the spin density distributed more broadly around both Co and Zr sites. NiVSn and NiTiSn illustrate contrasting cases: While NiVSn shows localized moments centered on the V atoms, NiTiSn exhibits more delocalized spin density around Ti, consistent with itinerant magnetism. The spin-density isosurfaces are shown in blue and red, representing negative and positive values of the same magnitude, respectively. In FeZrSb, the isosurface forms a compact, sphere-like shape tightly surrounding the Fe atoms, indicative of localized magnetism. For CoZrSn, the isosurface forms an extended, hollow network encompassing both Co and Zr atoms—a hallmark of itinerant

behavior. In NiVSn and NiTiSn, the isosurfaces around the V and Ti atoms are also roughly spherical, but their radii differ significantly: The larger isosurface radius in NiTiSn reflects its itinerant character, whereas the smaller, more localized red spheres in NiVSn resemble those of FeZrSb, indicating localized magnetism.

Overall, the observed trends in magnetic moment behavior reflect a delicate interplay between exchange splitting, electronic hybridization, and spin ordering in half-Heusler compounds. The pronounced collapse of magnetic moments in certain Co- and Rh-based systems underscores the role of itinerant magnetism, whereas the robustness of magnetism in Fe- and V-based compounds points to a more localized character. These insights deepen our understanding of magnetism in spin-gapped metallic half-Heuslers and provide a microscopic foundation for tailoring their electronic and magnetic properties in future spintronic applications.

B. Coulomb interaction parameters: Hubbard ${\cal U}$ and Hund exchange ${\cal J}$

To complement the analysis of magnetic moment behavior, we next examine the role of electronic correlations in shaping the magnetic properties of spin-gapped half-Heusler compounds. In particular, we focus on the effective on-site Coulomb interaction parameters—Hubbard U and Hund's exchange J-which serve as critical inputs for estimating the Stoner parameter I and evaluating ferromagnetic instability, as discussed in the next subsection. Since direct experimental determination of U and J is notoriously difficult and reliable data is limited, we computed these parameters from first principles using the constrained random phase approximation (cRPA) method implemented in the SPEX code, following the methodology outlined in Ref. [50] (see also Sec. III). The resulting U and J values for all compounds are summarized in Table II. where the slash separates the contributions associated with the d orbitals of the two transition metal elements, X and Y. These parameters are especially important in systems containing 3d, 4d, and 5d transition metals, which often exhibit strong electronic correlations. In such cases, beyond-DFT methods like DFT + U and DFT + DMFT have been shown to play an essential role in accurately describing the magnetic and electronic properties [56–59]. Heusler compounds, in particular, have been widely studied within this framework due to their rich correlation-driven physics [60,61].

With this approach, we obtain a consistent and physically meaningful set of U and J parameters for all investigated compounds. The computed Hubbard U values, which quantify the on-site Coulomb repulsion among d electrons, are broadly comparable to those of the corresponding elemental transition metals, typically ranging between 1.5 and 5.7 eV [62]. However, identifying systematic trends in the U values listed in Table II remains challenging, as U is known to depend sensitively on factors such as crystal symmetry, d-orbital filling, and hybridization effects. In the spin-gapped metallic half-Heuslers studied here, this complexity is amplified by the ternary nature of the unit cell, where hybridization between the d orbitals of the X and Y atoms, as well as the influence of the Z element, significantly affects the resulting Coulomb interactions—consistent with observations in Mn-based

TABLE II. Effective Coulomb interaction parameters (Hubbard U and Hund exchange J) for the valence d orbitals of transition metal atoms in the studied half-Heusler compounds, along with the estimated Stoner parameter I and the total density of states at the Fermi level $N(E_F)$ obtained from non-spin-polarized calculations. The product $I \times N(E_F)$ is presented as a direct measure of the Stoner instability, with an additional renormalized value $\alpha \times I \times N(E_F)$, where $\alpha = 0.6$ accounts for many-body effects (see text for details). The slash separates the values for the two transition metal atoms X and Y in the chemical formula of the compound. This dataset allows for a sublattice-resolved application of the Stoner criterion, distinguishing cases where both, one, or neither sublattice satisfies the condition for spontaneous magnetization.

XYZ	Orbitals	U (eV)	J (eV)	I (eV)	$N(E_F)$ (eV ⁻¹)	$I \times N(E_F)$	$\alpha \times I \times N(E_F)$
			spi	in-gapped metals			
FeZrSn	3d/4d	1.93/1.50	0.88/0.39	1.44/0.76	1.50/1.21	2.16/0.92	1.30/0.55
FeHfSn	3d/5d	2.08/1.40	0.89/0.36	1.48/0.71	1.28/0.76	1.84/0.54	1.14/0.32
FeTiSb	3d/3d	2.42/2.65	0.85/0.61	1.50/1.27	1.72/1.42	2.58/1.80	1.55/1.08
FeZrSb	3d/4d	2.73/1.75	0.90/0.37	1.62/0.79	1.75/0.62	2.84/0.49	1.70/0.29
FeHfSb	3d/5d	2.91/1.52	0.91/0.33	1.67/0.71	1.51/0.89	2.52/0.63	1.51/0.38
FeVSn	3d/3d	2.13/2.67	0.85/0.74	1.45/1.42	1.52/0.94	2.20/1.33	1.32/0.80
FeNbSn	3d/4d	2.20/1.96	0.89/0.47	1.51/0.96	1.50/0.53	2.27/0.51	1.36/0.31
FeTaSn	3d/5d	2.28/1.76	0.90/0.42	1.54/0.86	1.46/0.54	2.25/0.46	1.35/0.28
CoTiSn	3d/3d	2.33/2.11	0.94/0.63	1.59/1.17	1.07/1.45	1.70/1.70	1.02/1.02
CoZrSn	3d/4d	2.12/1.45	0.96/0.38	1.57/0.75	1.48/1.25	2.32/0.94	1.39/0.56
CoHfSn	3d/5d	2.58/1.39	0.98/0.36	1.70/0.70	1.15/0.92	1.96/0.64	1.17/0.39
RhTiSn	4d/3d	2.17/1.78	0.66/0.65	1.22/1.13	0.42/1.56	0.51/1.76	0.31/1.06
IrTiSn	5d/3d	1.89/1.86	0.58/0.65	1.08/1.15	0.39/1.49	0.42/1.71	0.25/1.03
NiTiIn	3d/3d	3.09/1.47	1.05/0.61	1.88/1.03	0.62/2.52	1.17/2.60	0.70/1.56
NiZrIn	3d/4d	3.00/1.23	1.07/0.39	1.89/0.72	0.60/1.56	1.13/1.12	0.68/0.67
PdTiIn	4d/3d	2.63/1.29	0.72/0.62	1.39/1.00	0.20/2.12	0.28/2.12	0.17/1.27
PtTiIn	5d/3d	2.28/1.41	0.65/0.52	1.23/0.90	0.30/2.50	0.37/2.25	0.22/1.35
CoVSb	3d/3d	3.65/3.14	0.94/0.71	1.85/1.48	0.98/4.36	1.81/6.45	1.09/3.87
RhVSb	4d/3d	2.90/3.00	0.65/0.73	1.36/1.48	0.37/3.68	0.50/5.45	0.30/3.27
IrVSb	5d/3d	2.62/3.12	0.58/0.73	1.22/1.50	0.17/2.13	0.21/3.20	0.12/1.92
PdTiSb	4d/3d	3.31/2.58	0.74/0.62	1.54/1.26	0.29/1.84	0.45/2.32	0.27/1.39
PtTiSb	5d/3d	2.85/2.48	0.64/0.58	1.33/1.19	0.28/3.29	0.37/3.90	0.22/2.35
NiVSn	3d/3d	4.15/2.71	1.04/0.72	2.08/1.40	0.69/2.74	1.44/3.84	0.86/2.30
NiVSb	3d/3d	3.95/2.82	1.02/0.69	2.02/1.39	1.52/7.51	3.07/10.4	1.84/6.26
				Gapped metals			
NiHfIn	3d/5d	3.37/1.20	1.09/0.37	1.98/0.68	0.50/1.30	0.99/0.88	0.59/0.53
CoNbSb	3d/4d	4.05/2.20	0.98/0.45	1.98/0.98	0.70/1.18	1.39/1.16	0.83/0.69
CoTaSb	3d/5d	4.08/1.93	0.98/0.39	1.99/0.86	0.56/0.76	1.11/0.65	0.67/0.39
NiTiSb	3d/3d	4.26/2.95	1.04/0.58	2.10/1.29	0.41/1.16	0.86/1.50	0.52/0.90
NiZrSb	3d/4d	4.82/1.96	1.08/0.36	2.27/0.82	0.27/0.47	0.61/0.39	0.37/0.23
NiHfSb	3d/5d	4.91/1.69	1.09/0.32	2.30/0.73	0.23/0.39	0.53/0.29	0.32/0.17
NiNbSn	3d/4d	4.72/2.19	1.09/0.46	2.25/0.99	0.62/1.30	1.40/1.29	0.84/0.77
NiTaSn	3d/5d	4.85/1.99	1.10/0.41	2.29/0.90	0.40/0.75	0.92/0.68	0.55/0.41

full-Heusler systems [50]. The calculated Hund's exchange J parameters are consistently smaller than their U counterparts, typically remaining below 1 eV. These values are in line with those reported for both elemental transition metals [62] and other Heusler compounds [49,50], further supporting the reliability of our cRPA-based results. In the following subsection, we use these parameters to estimate the Stoner criterion and assess the conditions under which ferromagnetic ordering becomes energetically favorable in spin-gapped half-Heusler compounds.

C. Stoner criterion and magnetic instabilities

The Stoner model provides a fundamental framework for understanding the onset of ferromagnetism in transitionmetal-based compounds by evaluating the instability of the nonmagnetic (NM) state toward spontaneous spin polarization. Its predictive power is particularly relevant for systems in which magnetism arises from an itinerant-electron mechanism, driven by electronic structure rather than localized moments. As seen in our analysis of FM and AFM magnetic moments (Sec. IV A) and electronic correlations (Sec. IV B), a clear distinction emerges between compounds exhibiting localized magnetism—such as those based on Fe and V—and those where magnetic moments are more itinerant, notably in Co-, Rh-, and Ni-based systems. For the latter group, the Stoner criterion serves as an effective tool to assess the tendency of the NM state to develop finite spin polarization. In contrast, for compounds with robust local moments stabilized by strong exchange interactions and Hund's coupling, the Stoner model alone is insufficient. In these cases, complementary local-moment-based approaches, such as Heisenberg

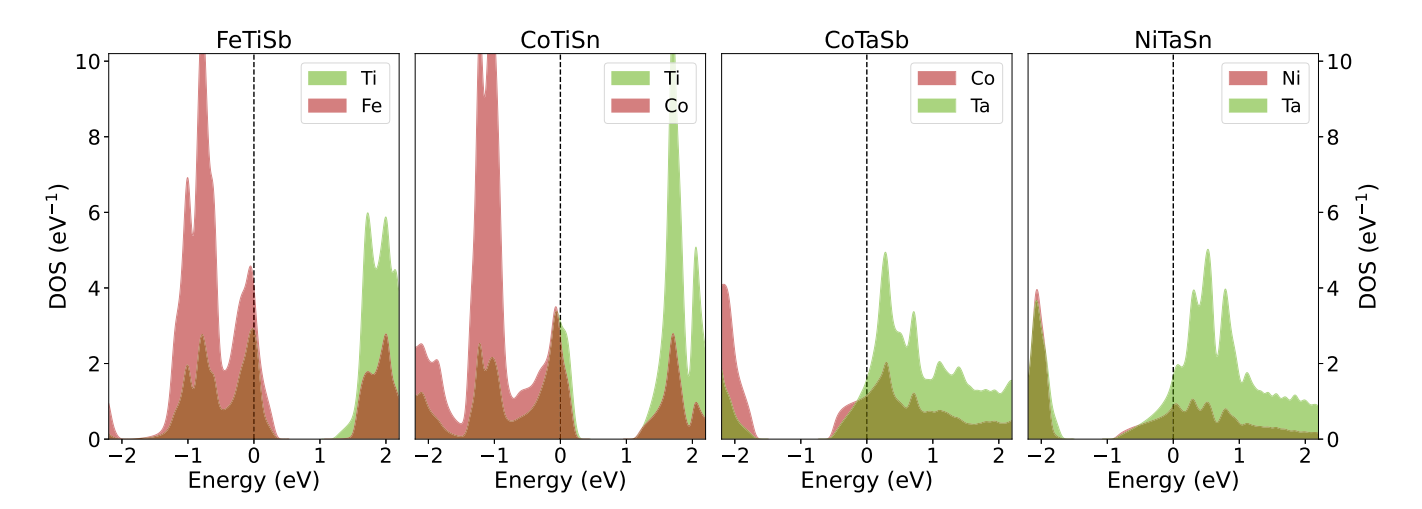


FIG. 4. Atom-resolved density of states (DOS) from nonmagnetic calculations for representative (spin)-gapped metallic half-Heusler compounds: FeTiSb, CoTiSn, CoTaSb, and NiTaSn. For FeTiSb and CoTiSn, both X-Y sublattices (Fe-Ti and Co-Ti, respectively) exhibit high DOS at the Fermi level, indicating that the Stoner criterion is satisfied. In contrast, for CoTaSb and NiTaSn, the corresponding X-Y sublattices (Co-Ta and Ni-Ta) show low DOS at the Fermi level, consistent with the absence of magnetic ordering. The DOS is plotted in the energy range $E_F \pm 2$ eV, and the atom-resolved curves represent the sum of spin-up and spin-down contributions; therefore, the values should be divided by two when applied to the Stoner criterion.

exchange models, are also required to capture the underlying magnetic behavior.

To quantitatively assess the applicability of the Stoner model to the half-Heusler compounds studied here, we use the effective Coulomb interaction parameters (Hubbard Uand Hund's exchange J) obtained in the previous subsection to estimate the Stoner parameter I (see Table II). The Stoner parameter is computed using the mean-field expression proposed by Stollhoff *et al.*, given by I = (U + 6J)/5 [51]. This relation, derived from the Hartree-Fock solution of the multi-orbital Hubbard model, has been shown to yield reliable results for transition-metal systems and reproduces the Stoner parameters of elemental 3d materials with good accuracy. To evaluate magnetic stability, we also calculated the total density of states at the Fermi level $N(E_F)$ in the nonmagnetic (NM) state and determined the Stoner product $I \times N(E_F)$. According to the conventional criterion, a compound is predicted to be ferromagnetic when $I \times N(E_F) > 1$. For systems with two different transition-metal atoms, such as FeVSn or CoVSb, this condition must be evaluated separately for each sublattice, since the original Stoner model was formulated for a single magnetic species. These materials can be treated as two-sublattice magnets, where each sublattice corresponds to one of the transition-metal atoms. Accordingly, the instability conditions become

$$I_X \times N_X(E_F) > 1$$
, $I_Y \times N_Y(E_F) > 1$,

where I_X and I_Y are the Stoner parameters for the two sublattices, and $N_X(E_F)$ and $N_Y(E_F)$ are the corresponding projected DOS at the Fermi level. If both conditions are satisfied, magnetic moments are expected on both sublattices. If only one is satisfied, magnetism is likely to be localized on that sublattice, while the other remains nonmagnetic or possesses a small induced spin magnetic moment due to hybridization effects between orbitals sitting at neighboring atoms and transforming with the same symmetry (e.g., Zr in FeZrSb). If neither

inequality holds, the system is expected to remain nonmagnetic, in agreement with our DFT results.

As examples of the interplay between the appearance of magnetic order and the DOS, we present in Fig. 4 the atomresolved DOS for FeTiSb and CoTiSn, which are found to be spin-gapped metals, and CoTaSb and NiTaSn, which are found to be normal nonmagnetic gapped metals (see Table II). In the case of the former FeTiSb and CoTiSn compounds, both *X* and *Y* sublattices exhibit pronounced DOS at the Fermi level, consistent with the Stoner criterion being satisfied and the presence of magnetic instabilities leading to magnetic order. In contrast, for CoTaSb and NiTaSn, the *X* and *Y* sublattices show very low DOS at the Fermi level, in agreement with the absence of magnetism in these compounds.

It is worth noting that the analysis above neglects manybody correlation effects, which are known to reduce the effective Stoner parameter I by suppressing local charge and spin fluctuations. According to Ref. [51], such correlations can lower I by as much as 30–40% in 3d transition metals, where the narrow d bands and localized orbitals enhance fluctuations. To account for this, we also consider a renormalized version of the criterion, $\alpha \times I \times N(E_F)$ with $\alpha = 0.6$, which provides a more realistic estimate of magnetic instability in 3d-dominated systems. However, this $\alpha = 0.6$ value is not universal. In 4d and 5d transition metals, the valence d orbitals are more spatially extended, the d bands are broader, and the hybridization with ligand states is stronger. These factors enhance electronic screening and reduce the impact of local correlations, so that the suppression of I is weaker and α can approach unity (see e.g., fcc Pd in Ref. [63]). To the best of our knowledge, there is no practical way to compute element- and compound-specific α values without an explicit treatment of spin fluctuations beyond the scope of the present work. Therefore, in Table II we report both the bare Stoner product $IN(E_F)$ ($\alpha = 1$) and the renormalized values with $\alpha = 0.6$. For compounds with 4d or 5d sublattices, the actual α is expected to be larger than 0.6, and thus their magnetic

tendency could be underestimated by the renormalized criterion. A notable example is NiZrIn and FeZrSn, where the Zr-4d Stoner products are close to unity (1.12 and 0.92, respectively). While the renormalized values drop to 0.67 and 0.55, these should be interpreted with caution: For the Zr-4d states, the effective α is likely closer to one, so that the proximity to magnetism may in fact be stronger than the renormalized criterion suggests.

Our calculations reveal three distinct types of magnetic behavior among the half-Heusler compounds, classified according to whether the Stoner criterion is satisfied on one, both, or neither of the transition-metal sublattices. In compounds such as FeTiSb, FeVSn, CoTiSn, and CoVSb, both transition-metal atoms satisfy the Stoner condition, resulting in finite magnetic moments on both sublattices. In a second group of systems, only one sublattice meets the criterion, leading to magnetism localized on a single atomic site. For example, in RhTiSn and PdTiIn, the Ti atom develops a sizable magnetic moment, while the Rh and Pd atoms remain nonmagnetic because of their low projected DOS at the Fermi level, which fails to induce spin instability. For FeZrSb, only Fe atoms satisfy the Stoner criterion, presenting a large value of spin magnetic moment while Zr atoms, which do not satisfy the Stoner criterion, present a much smaller spin magnetic moment induced by the Fe atomic spin magnetic moments. The third group comprises materials in which neither sublattice satisfies the Stoner criterion, leading to a nonmagnetic ground state. These compounds, which we classify as gapped metals, include NiHfIn, CoNbSb, CoTaSb, NiTiSb, NiZrSb, NiHfSb, NiNbSn, and NiTaSn. Despite their metallic character, these systems exhibit a strongly reduced total DOS at the Fermi level, which suppresses magnetic instability. In all such cases, both the unrenormalized and renormalized Stoner products, $I \times N(E_F)$ and $\alpha \times I \times N(E_F)$, remain below the critical threshold of unity. The absence of magnetism in these materials is primarily attributed to strong hybridization effects and electronic band structure features that lower the DOS at E_F . This sets them apart from nearly ferromagnetic metals such as Pd, where a high DOS near the Fermi level leads to strong spin fluctuations and exchange-enhanced paramagnetism.

Despite the widespread use of the Stoner model for predicting magnetism in transition-metal-based systems, a fully developed multisublattice extension remains lacking. Lichtenstein et al. [64] proposed an advanced theoretical framework that combines Stoner, Heisenberg, and Hubbard concepts through a site- and orbital-resolved spin-fluctuation theory within the LDA + DMFT formalism. While this approach does not explicitly define a sublattice-resolved Stoner criterion in the conventional sense, it provides strong conceptual justification for evaluating magnetic instabilities on inequivalent atomic sites individually. Our results demonstrate that such a sublattice-based application of the Stoner criterion is highly effective in capturing the diverse magnetic behavior observed in half-Heusler compounds, particularly in systems exhibiting a coexistence of localized and itinerant magnetism. Nevertheless, for materials with strong local moments or complex magnetic interactions, additional theoretical treatments—such as Heisenberg exchange modeling or beyond-DFT approaches—are likely necessary to achieve a more comprehensive description. Future developments incorporating many-body techniques, such as DMFT or *GW*-based corrections, hold promise for refining our understanding of magnetic phase stability and correlation-driven phenomena in these complex intermetallics.

D. Magnetic interactions, spin-wave properties, and Curie temperatures

Following the analysis of magnetic moments and Stoner instabilities presented in the previous sections, we now turn to the computation of magnetic exchange interactions, Curie temperatures, and spin-wave spectra to complete the theoretical picture of magnetism in spin-gapped half-Heusler compounds. These quantities are essential for assessing the stability of magnetic order and the nature of low-energy excitations, both of which are critical for potential spintronic applications. Our approach follows the standard methodology of mapping ab initio total-energy calculations onto a classical Heisenberg Hamiltonian [54,65–68]. This approximation is well justified for systems with localized magnetic moments and can still yield meaningful insights for moderately itinerant magnets, provided the magnetic moments are not too small. However, in strongly itinerant systems, the accuracy of the Heisenberg mapping becomes limited. In addition, the calculation of spin-wave dispersions captures only collective excitations and neglects so-called Stoner excitations—singleparticle spin-flip processes that can lead to Landau damping. This simplification is reasonable in half-metallic systems, where spin flips are energetically suppressed due to the position of the Fermi level relative to the minority-spin conduction band edge. Finally, Curie temperatures are estimated using the mean-field approximation (MFA) applied to the computed exchange parameters. While MFA provides qualitative trends, it is known to systematically overestimate the actual transition temperatures by neglecting collective spin fluctuations. More accurate estimates would require approaches such as the random phase approximation (RPA), which includes spin-wave renormalization effects.

With these considerations in mind, we now proceed to the evaluation of exchange constants, which form the basis for our analysis of magnetic excitations and thermal stability. As described in Sec. III, the exchange interactions are computed using the real-space LKAG formalism, which maps the results of ab initio electronic structure calculations onto a classical Heisenberg Hamiltonian in a linear-response framework. In magnetic systems such as half-Heusler compounds, two primary mechanisms contribute to the exchange interactions: direct and indirect exchange [69]. The direct exchange arises from interactions between magnetic atoms on different sublattices—typically when both transition metal atoms are magnetic and occupy nearest-neighbor positions. These intersublattice interactions are especially relevant in compounds with multiple magnetic species. The indirect exchange, by contrast, takes place between magnetic atoms of the same type within a single sublattice. It is mediated by conduction electrons and is often described by Ruderman-Kittel–Kasuya–Yosida (RKKY)–like mechanisms. In systems for which only one sublattice hosts magnetic moments, the stability of the magnetic phase is governed primarily by these

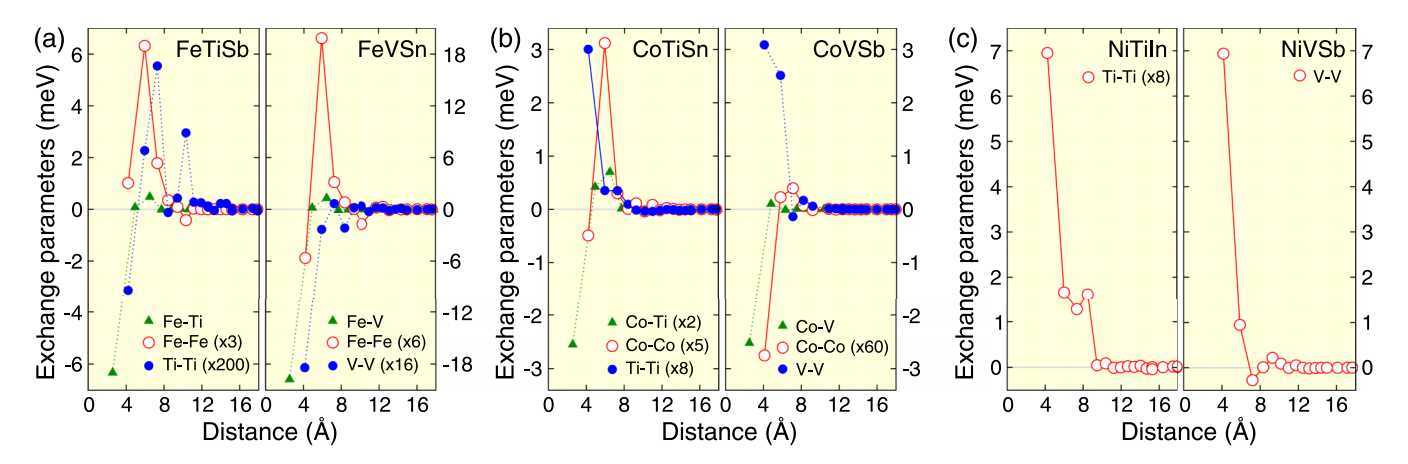


FIG. 5. Intra- and intersublattice Heisenberg exchange parameters as a function of interatomic distance for six representative spin-gapped metallic half-Heusler compounds: (a) FeTiSb and FeVSn, (b) CoTiSn and CoVSb, and (c) NiTiSn and NiVSb. Each curve corresponds to exchange interactions between specific magnetic atoms. In several cases, the exchange constants have been multiplied by an integer factor (indicated in parentheses in the legend) to enhance visibility.

intrasublattice interactions. The relative strength and sign of the direct and indirect exchange contributions determine the nature of the magnetic ground state and are key factors in establishing the Curie temperature and spin-wave behavior of the system.

Figure 5 presents the calculated exchange constants as a function of interatomic distance for six representative half-Heusler compounds. For FeTiSb and FeVSn, both with 17 valence electrons per formula unit, the dominant magnetic interaction is the direct intersublattice exchange between Fe and Ti (or V) atoms. This coupling is negative for nearest neighbors, favoring antiparallel alignment—consistent with the spin magnetic moments reported in Table I, where Fe and Ti(V) moments are oriented oppositely. In contrast, the intrasublattice interactions (Fe–Fe and Ti–Ti or V–V) are significantly weaker; to enhance their visibility in the plot, we scaled them by factors of 3 and 6 for Fe–Fe, and 200 and 16 for Ti–Ti and V–V, respectively.

The compounds CoTiSn and CoVSb illustrate contrasting magnetic behavior. CoTiSn exhibits itinerant magnetism, with magnetism primarily driven by Co-Ti exchange. Although the nearest-neighboring Co-Ti interaction is negative as shown in Fig. 5, the overall Co-Ti exchange interaction is positive favoring ferromagnetic alignment of the spin magnetic moments. This is because of the fact that the next-nearest neighboring interactions are positive and the number of second Co-Ti neighbors is much larger than the number of the nearest Co-Ti neighbors. The Ti-Ti interactions are much weaker, indicating limited magnetic contribution from the Ti sublattice. CoVSb, on the other hand, shows more localized magnetism, with V–V interactions that are comparable in strength to the Co– V exchange. This reflects a cooperative magnetic ordering involving both sublattices and is supported by the data in Table I, where V atoms carry magnetic moments nearly an order of magnitude larger than those on Co.

The final two compounds, NiTiSn and NiVSb, demonstrate magnetism localized predominantly on the Ti and V sublattices, respectively. In NiVSb, the large spin magnetic moments on V atoms (approximately $2\,\mu_B)$ are accompanied by strong V–V exchange constants, indicating robust

local-moment magnetism. In contrast, NiTiSn displays smaller and more delocalized Ti moments, resulting in significantly weaker Ti–Ti exchange. These findings highlight the diverse nature of magnetic exchange interactions across the half-Heusler family, governed by both electronic structure and sublattice contributions.

The exchange constants discussed above were subsequently used to estimate the Curie temperatures, as outlined in Sec. III. The resulting $T_{\rm C}$ values are presented in the last column of Table I. For most compounds, the Curie temperatures lie below room temperature. This is especially true for itinerant magnets, where $T_{\rm C}$ values often fall below 100 K, reflecting the weaker exchange interactions associated with delocalized magnetic moments. In contrast, several compounds exhibiting localized magnetism show significantly higher Curie temperatures, making them promising candidates for spintronic applications. Notably, FeVSn, CoVSb, and NiVSb exhibit $T_{\rm C}$ values of 532 K, 419 K, and 684 K, respectively.

This trend can be qualitatively understood in terms of an empirical rule suggesting that the Curie temperature scales with the sum of the absolute values of the atomic spin magnetic moments [70,71]. For example, in FeVSn, although the total spin moment is only $-0.88\,\mu_{\rm B}$ beause of antiparallel alignment between Fe and V, the sum of the absolute moments is $2.88\,\mu_{\rm B}$. Similarly, the corresponding values are $1.74\,\mu_{\rm B}$ for CoVSb and $2.15\,\mu_{\rm B}$ for NiVSb. While this empirical trend aligns with the relatively high $T_{\rm C}$ values in these cases, it should be emphasized that there is no strict linear relationship, and the applicability of this rule remains limited.

Finally, we briefly comment on the expected electronic behavior of spin-gapped metals above $T_{\rm C}$. In conventional magnetic metals, the loss of magnetic order typically results in a paramagnetic metallic state. In contrast, the spin-gapped systems studied here may retain a gapped character even in the nonmagnetic state, depending on the symmetry of the spin-resolved band structure. This scenario is particularly likely when both spin channels exhibit the same carrier type (either p type or n type), as shown in Figs. 1(d) and 1(e), or when one spin channel remains semiconducting. In such cases, the

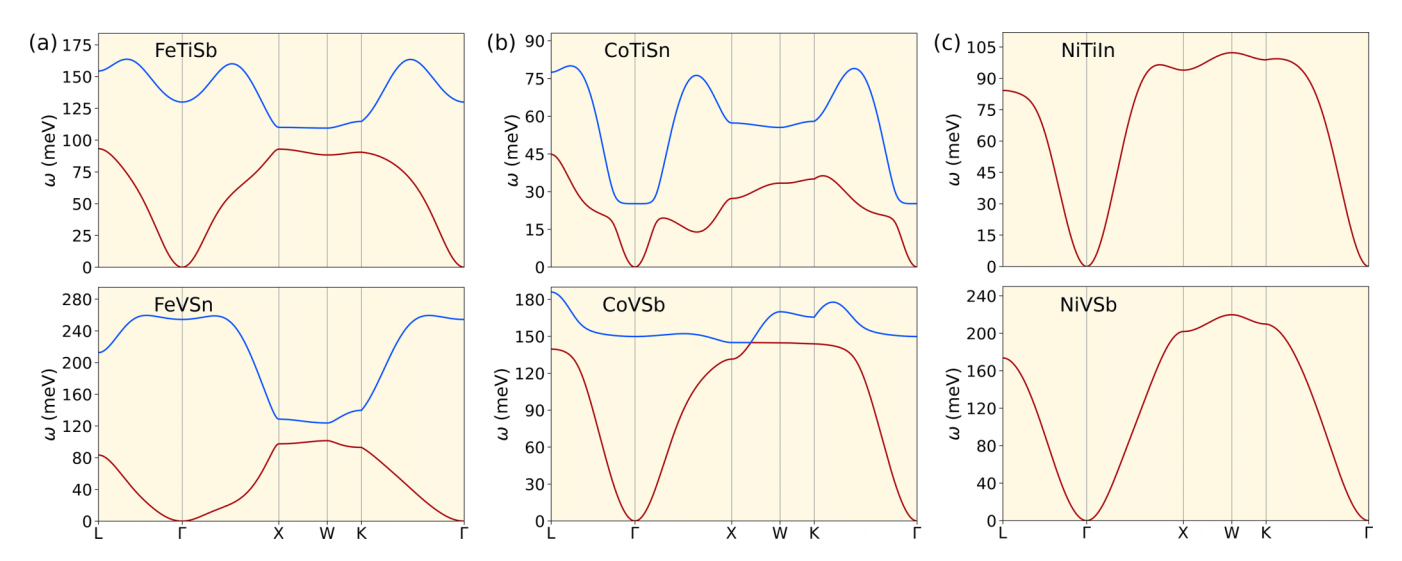


FIG. 6. Calculated magnon dispersion curves for six representative half-Heusler compounds: (a) FeTiSb and FeVSn, (b) CoTiSn and CoVSb, and (c) NiTiSn and NiVSb. In compounds with only one magnetic atom per formula unit (NiTiSn and NiVSb) the spectra consist of a single acoustic magnon branch (red curve). In contrast, the other four compounds contain two magnetic atoms per unit cell, resulting in both an acoustic branch (red curve) and a higher-energy optical magnon branch (blue curve). Among them, CoTiSn exhibits ferromagnetic ordering, while FeTiSb, FeVSb, and CoVSb are ferrimagnets with antiparallel sublattice moments. All magnon spectra are plotted along the high-symmetry path L-Γ-X-W-K-Γ in the Brillouin zone, with energy given in meV.

paramagnetic state may closely resemble a gapped metal rather than a conventional one. On the other hand, spin-gapped metals with mixed p- and n-type character [Fig. 1(f)] are expected to evolve into ordinary paramagnetic metals above T_C .

In addition to determining Curie temperatures, the exchange constants also allow us to investigate the dynamical magnetic excitations of the system—specifically, the magnon spectra, as discussed in Sec. III. Magnons, or spin-wave excitations, represent the low-energy collective modes of the spin system and are distinct from single-particle spin-flip excitations known as Stoner excitations. Figure 6 shows the calculated magnon spectra for six representative compounds, illustrating how the number of magnetic sublattices and the nature of magnetic ordering influence the spin-wave dispersion.

NiTiSn and NiVSb each have only one magnetic sublattice (Ti and V, respectively), resulting in a single acoustic magnon branch. This is true despite their differing magnetic character—NiTiSn being an itinerant magnet and NiVSb a localized one. In contrast, FeTiSb, FeVSb, CoTiSn, and CoVSb feature two magnetic sublattices, leading to both acoustic and optical magnon branches. The acoustic mode corresponds to in-phase precession of the sublattice moments, while the optical mode involves out-of-phase precession and appears at higher energy. Among these compounds, only CoTiSn exhibits ferromagnetic alignment with parallel sublattice moments, whereas the others show ferrimagnetic coupling with antiparallel alignment. This distinction influences both the energy separation and intensity distribution between the two magnon branches.

Despite differences in spectral features, the acoustic mode consistently vanishes at the Γ point for all systems, as expected from the Goldstone theorem in the absence of spin-orbit coupling. Near the zone center, the dispersion follows a quadratic form $E(\mathbf{q}) = D \cdot |\mathbf{q}|^2$, where D is the spin-wave

stiffness constant. The calculated D values, listed in Table I, span a wide range from 165 to 936 meV $Å^2$, reflecting the diversity of exchange interactions and the localized versus itinerant nature of magnetism across the studied half-Heusler compounds.

While linear spin-wave theory based on DFT-calculated exchange parameters yields valuable insights into collective magnetic excitations, it has inherent limitations when applied to metallic systems. In particular, the classical Heisenberg model employed here neglects the coupling between collective magnons and single-particle spin-flip (Stoner) excitations. which can result in significant damping of spin waves. This limitation is especially relevant for spin-gapped metallic systems, where the Fermi level may lie close to the onset of the spin-flip continuum. As a result, our current method does not account for Landau damping effects or finite magnon lifetimes that arise from such interactions. A more rigorous treatment would require going beyond the Heisenberg model and employing approaches such as time-dependent density functional theory (TDDFT) or many-body perturbation theory (MBPT), which explicitly account for dynamic electron-hole correlations [72–78].

These limitations are particularly pertinent for compounds in which one or both spin channels exhibit *p*-type spin-gapped metallic behavior, such as FeVSb, where the Fermi level lies close to the minority-spin conduction band edge. In such cases, efficient magnon–Stoner coupling can lead to pronounced damping and short magnon lifetimes. In contrast, compounds like CoVSb and NiVSb, where one spin channel displays *n*-type spin-gapped metallic behavior and the other is semiconducting, are expected to exhibit more coherent and long-lived magnons because of the presence of a Stoner gap that separates collective modes from the spin-flip continuum. Similar behavior may also arise in Fe- and Ti-based half-Heuslers with a full semiconducting gap in one spin channel,

as indicated in Table I. Understanding how the type and size of the spin-gap affect magnon coherence and damping remains an important open question, with direct implications for the design of next-generation spintronic and magnonic devices based on spin-gapped metallic half-Heuslers.

V. SUMMARY AND CONCLUSIONS

In this work, we presented a comprehensive first-principles investigation of spin-gapped metallic half-Heusler compounds, with the goal of uncovering the microscopic origin of magnetism and its implications for spintronic applications. Using multiple ab initio electronic structure methods, we systematically explored the nature of magnetic moments, the role of electronic correlations, and the resulting exchange interactions across a broad family of compounds with 16, 17, 19, or 20 valence electrons per formula unit. Our analysis of ferro-, ferri-, and antiferromagnetic configurations revealed that Co- and Ni-based systems predominantly exhibit itinerant magnetism, while Fe-, Ti-, and V-based compounds display a richer spectrum, ranging from localized to itinerant behavior—and in some cases, a coexistence of both. Spin-density isosurface plots further corroborate these trends, distinguishing localized from delocalized spin polarization in real space.

To elucidate the origin of magnetism, we estimated the Stoner parameter I from cRPA-calculated Hubbard U and Hund's exchange J values. This enabled a material-specific application of the Stoner criterion, which successfully accounts for the emergence of magnetism in many itinerant systems, as well as the absence of magnetic order in several Co- and Ni-based compounds. In the latter case, strong hybridization and a low DOS at the Fermi level suppress the Stoner instability, despite the presence of transition metal elements.

We computed Heisenberg exchange parameters using the LKAG formalism, which allowed us to estimate Curie temperatures and analyze spin-wave spectra. Depending on the magnetic sublattice configuration, magnetic order is stabilized either through intersublattice (direct) or intrasublattice (indirect) exchange interactions. In compounds where both sublattices carry substantial spin moments, the Curie temperatures exceed room temperature, identifying them as promising candidates for high-temperature spintronic applications. The calculated magnon spectra exhibit well-defined acoustic modes and, in multisublattice systems, additional optical branches. The spin-wave stiffness constants span a wide range, reflecting the diversity of magnetic behavior across the half-Heusler family.

Overall, our study offers fundamental insights into the delicate interplay between localized and itinerant magnetism in spin-gapped metallic half-Heusler compounds. By integrating advanced electronic structure methods with analytical modeling, we construct a comprehensive theoretical framework for understanding the microscopic origins of magnetic order in these systems. This framework paves the way for the predictive design of spintronic materials with precisely engineered magnetic and transport properties. In particular, the coexistence of spin-resolved energy gaps and tunable magnetism uniquely positions spin-gapped metals as promising platforms for next-generation electronic applications, including multifunctional steep-slope field-effect transistors and other beyond-CMOS devices.

ACKNOWLEDGMENTS

This work was supported by several funding sources, including SFB CRC/TRR 227 and SFB 1238 (Project No. C01) of the Deutsche Forschungsgemeinschaft (DFG), the European Union (EFRE) through Grant No: ZS/2016/06/79307, and the Federal Ministry of Education and Research of Germany (BMBF) within the framework of the Palestinian-German Science Bridge (BMBF Grant No. DBP01436). M.T. acknowledges the TUBITAK ULAKBIM, High Performance and Grid Computing Center (TRUBA resources). S.G. acknowledges National Supercomputing Mission (NSM) for providing computing resources of 'PARAM SEVA' at IIT, Hyderabad, which is implemented by C-DAC and supported by the Ministry of Electronics and Information Technology (MeitY) and Department of Science and Technology (DST), Government of India. B.S. acknowledges financial support from Swedish Research Council (Grant No. 2022-04309) and STINT Mobility Grant for Internationalization (Grant No. MG2022-9386). The computations were enabled by resources provided by the National Academic Infrastructure for Supercomputing in Sweden (NAISS) at NSC and PDC (NAISS 2024/3-40) partially funded by the Swedish Research Council through Grant Agreement No. 2022-06725.

DATA AVAILABILITY

The data that support the findings of this article are not publicly available upon publication because it is not technically feasible and/or the cost of preparing, depositing, and hosting the data would be prohibitive within the terms of this research project. The data are available from the authors upon reasonable request.

A. Hirohata, K. Yamada, Y. Nakatani, I.-L. Prejbeanu, B. Diény, P. Pirro, and B. Hillebrands, Review on spintronics: Principles and device applications, J. Magn. Magn. Mater. 509, 166711 (2020).

^[2] S. Tavares, K. Yang, and M. A. Meyers, Heusler alloys: Past, properties, new alloys, and prospects, Prog. Mater. Sci. 132, 101017 (2023).

^[3] Snehashish Chatterjee, Souvik Chatterjee, S. Giri, and S. Majumdar, Transport properties of Heusler compounds

and alloys, J. Phys.: Condens. Matter **34**, 013001 (2022).

^[4] T. Graf, C. Felser, and S. S. P. Parkin, Simple rules for the understanding of Heusler compounds, Prog. Solid State Chem. **39**, 1 (2011).

^[5] S. V. Faleev, Y. Ferrante, J. Jeong, M. G. Samant, B. Jones, and S. S. P. Parkin, Heusler compounds with perpendicular magnetic anisotropy and large tunneling magnetoresistance, Phys. Rev. Mater. 1, 024402 (2017).

- [6] Q. Gao, I. Opahle, and H. Zhang, High-throughput screening for spin-gapless semiconductors in quaternary Heusler compounds, Phys. Rev. Mater. 3, 024410 (2019).
- [7] J. Ma, V. I. Hegde, K. Munira, Y. Xie, S. Keshavarz, D. T. Mildebrath, C. Wolverton, A. W. Ghosh, and W. H. Butler, Computational investigation of half-Heusler compounds for spintronics applications, Phys. Rev. B 95, 024411 (2017).
- [8] M. Marathe and H. C. Herper, Exploration of all-3d Heusler alloys for permanent magnets: An *ab initio* based high-throughput study, Phys. Rev. B 107, 174402 (2023).
- [9] S. Sanvito, J. Xue, A. Tiwari, M. Zic, T. Archer, P. Tozman, M. Venkatesan, M. Coey, and S. Curtarolo, Accelerated discovery of new magnets in the Heusler alloy family, Sci. Adv. 3, e1602241 (2017).
- [10] S. Ouardi, G. H. Fecher, C. Felser, and J. Kübler, Realization of spin gapless semiconductors: The Heusler compound Mn₂CoAl, Phys. Rev. Lett. 110, 100401 (2013).
- [11] I. Galanakis, K. Özdoğan, and E. Şaşıoğlu, A proposal for an alternative class of spin filter materials: Hybridization-induced high-T_C ferromagnetic semiconductors CoVXAl (X = Ti, Zr, Hf), Appl. Phys. Lett. 103, 142404 (2013).
- [12] I. Galanakis, K. Özdoğan, and E. Şaşıoğlu, High-T_C fully compensated ferrimagnetic semiconductors as spin-filter materials: The case of CrVXAl (X = Ti, Zr, Hf) Heusler compounds, J. Phys.: Condens. Matter 26, 086003 (2014).
- [13] S.-Y. Lin, M. Chen, X.-B. Yang, Y.-J. Zhao, S.-C. Wu, C. Felser, and B. Yan, Theoretical search for half-Heusler topological insulators, Phys. Rev. B 91, 094107 (2015).
- [14] Z. Wang, M. G. Vergniory, S. Kushwaha, M. Hirschberger, E. V. Chulkov, A. Ernst, N. P. Ong, R. J. Cava, and B. A. Bernevig, Time-reversal-breaking Weyl fermions in magnetic Heusler alloys, Phys. Rev. Lett. 117, 236401 (2016).
- [15] K. Manna, Y. Sun, L. Muechler, J. Kübler, and C. Felser, Heusler, Weyl and Berry, Nat. Rev. Mater. 3, 244 (2018).
- [16] H. Liu, J. Liang, T. Sun, and L. Wang, Recent progress in topological semimetal and its realization in Heusler compounds, Mater. Today Phys. 41, 101343 (2024).
- [17] S. Chadov, S.-C. Wu, C. Felser, and I. Galanakis, Stability of Weyl points in magnetic half-metallic Heusler compounds, Phys. Rev. B **96**, 024435 (2017).
- [18] D. Jung, H.-J. Koo, and M.-H. Whangbo, Study of the 18-electron band gap and ferromagnetism in semi-Heusler compounds by non-spin-polarized electronic band structure calculations, J. Mol. Struct. 527, 113 (2000).
- [19] J. Pierre, R. V. Skolozdra, Y. K. Gorelenko, and M. Kouacou, From nonmagnetic semiconductor to itinerant ferromagnet in the TiNiSn-TiCoSn series, J. Magn. Magn. Mater. 134, 95 (1994).
- [20] J. Toboła and J. Pierre, Electronic phase diagram of the XTZ (X = Fe, Co, Ni; T = TI, V, Zr, Nb, Mn; Z = SN, Sb) semi-Heusler compounds, J. Alloys Compd. **296**, 243 (2000).
- [21] S. Ouardi, G. H. Fecher, C. Felser, M. Schwall, S. S. Naghavi, A. Gloskovskii, B. Balke, J. Hamrle, K. Postava, J. Pištora, S. Ueda, and K. Kobayashi, Electronic structure and optical, mechanical, and transport properties of the pure, electron-doped, and hole-doped Heusler compound CoTiSb, Phys. Rev. B 86, 045116 (2012).
- [22] M. Mokhtari, F. Dahmane, G. Benabdellah, L. Zekri, S. Benalia, and N. Zekri, Theoretical study of the structural stability, electronic and magnetic properties of XVSb (X = Fe, Co, and

- Ni) half-Heusler compounds, Condens. Matter Phys. **21**, 43705 (2018).
- [23] E. Gürbüz, S. Ghosh, E. Şaşıoğlu, I. Galanakis, I. Mertig, and B. Sanyal, Spin-polarized two-dimensional electron/hole gas at the interface of nonmagnetic semiconducting half-Heusler compounds: Modified Slater-Pauling rule for half-metallicity at the interface, Phys. Rev. Mater. 7, 054405 (2023).
- [24] E. Gürbüz, M. Tas, E. Şaşıoğlu, I. Mertig, B. Sanyal, and I. Galanakis, First-principles prediction of energy bandgaps in 18-valence electron semiconducting half-Heusler compounds: Exploring the role of exchange and correlation, J. Appl. Phys. 134, 205703 (2023).
- [25] G. Xu, E. K. Liu, Y. Du, G. J. Li, G. D. Liu, W. H. Wang, and G. H. Wu, New spin gapless semiconductors family: Quaternary Heusler compounds, Europhys. Lett. **102**, 17007 (2013).
- [26] E. Şaşıoğlu, M. Tas, S. Ghosh, W. Beida, B. Sanyal, S. Blügel, I. Mertig, and I. Galanakis, Spin gapped metals: A novel class of materials for multifunctional spintronic devices, J. Magn. Magn. Mater. 615, 172792 (2025).
- [27] K. Sato, L. Bergqvist, J. Kudrnovský, P. H. Dederichs, O. Eriksson, I. Turek, B. Sanyal, G. Bouzerar, H. Katayama-Yoshida, V. A. Dinh, T. Fukushima, H. Kizaki, and R. Zeller, First-principles theory of dilute magnetic semiconductors, Rev. Mod. Phys. 82, 1633 (2010).
- [28] B.-H. Lei and D. J. Singh, Computational search for itinerant n-type and p-type magnetic semiconductors: Arsenopyrites as bipolar magnetic semiconductors, Phys. Rev. B 105, L121201 (2022).
- [29] N. T. Tu, P. N. Hai, L. D. Anh, and M. Tanaka, (GA,Fe)Sb: A *p*-type ferromagnetic semiconductor, Appl. Phys. Lett. **105**, 132402 (2014).
- [30] K. Kroth, B. Balke, G. H. Fecher, V. Ksenofontov, C. Felser, and H.-J. Lin, Diluted magnetic semiconductors with high Curie temperature based on C1(b) compounds: COTi_{1-x}Fe_xSb, Appl. Phys. Lett. 89, 202509 (2006).
- [31] E. Şaşıoğlu, P. Bodewei, N. F. Hinsche, and I. Mertig, Multifunctional steep-slope spintronic transistors with spingapless-semiconductor or spin-gapped-metal electrodes, Phys. Rev. Appl. 23, 044022 (2025).
- [32] https://oqmd.org/.
- [33] J. Saal, S. Kirklin, M. Aykol, B. Meredig, and C. Wolverton, Materials design and discovery with high-throughput density functional theory: The open quantum materials database (OQMD), JOM 65, 1501 (2013).
- [34] S. Kirklin, J. Saal, B. Meredig, A. Thompson, J. Doak, M. Aykol, S. Rühl, and C. Wolverton, The open quantum materials database (OQMD): Assessing the accuracy of DFT formation energies, npj Comput. Mater. 1, 15010 (2015).
- [35] J. P. Perdew, K. Burke, and M. Ernzerhof, Generalized gradient approximation made simple, Phys. Rev. Lett. 77, 3865 (1996).
- [36] K. Lejaeghere *et al.*, Reproducibility in density functional theory calculations of solids, Science **351**, aad3000 (2016).
- [37] J. W. Furness, A. D. Kaplan, J. Ning, J. P. Perdew, and J. Sun, Accurate and numerically efficient r²SCAN meta-generalized gradient approximation, J. Phys. Chem. Lett. **11**, 8208 (2020).
- [38] S. Smidstrup, D. Stradi, J. Wellendorff, P. A. Khomyakov, U. G. Vej-Hansen, M.-E. Lee, T. Ghosh, E. Jónsson, H. Jónsson, and K. Stokbro, First-principles Green's-function method for surface calculations: A pseudopotential localized basis set approach, Phys. Rev. B 96, 195309 (2017).

- [39] S. Smidstrup, T. Markussen, P. Vancraeyveld, J. Wellendorff, J. Schneider, T. Gunst, B. Verstichel, D. Stradi, P. A. Khomyakov, U. G. Vej-Hansen, *et al.*, QuantumATK: An integrated platform of electronic and atomic-scale modeling tools, J. Phys.: Condens. Matter 32, 015901 (2020).
- [40] M. J. van Setten, M. Giantomassi, E. Bousquet, M. J. Verstraete, D. R. Hamann, X. Gonze, and G. M. Rignanese, The PSEUDODOJO: Training and grading a 85 element optimized norm-conserving pseudopotential table, Comput. Phys. Commun. 226, 39 (2018).
- [41] H. J. Monkhorst and J. D. Pack, Special points for Brillouinzone integrations, Phys. Rev. B 13, 5188 (1976).
- [42] A. I. Liechtenstein, M. I. Katsnelson, V. P. Antropov, and V. A. Gubanov, Local spin density functional approach to the theory of exchange interactions in ferromagnetic metals and alloys, J. Magn. Magn. Mater. 67, 65 (1987).
- [43] X. He, N. Helbig, M. J. Verstraete, and E. Bousquet, TB2J: A python package for computing magnetic interaction parameters, Comput. Phys. Commun. 264, 107938 (2021).
- [44] M. Pajda, J. Kudrnovský, I. Turek, V. Drchal, and P. Bruno, *Ab initio* calculations of exchange interactions, spin-wave stiffness constants, and Curie temperatures of Fe, Co, and Ni, Phys. Rev. B **64**, 174402 (2001).
- [45] D. Wortmann, G. Michalicek, N. Baadji, M. Betzinger, G. Bihlmayer, J. Bröder, T. Burnus, J. Enkovaara, F. Freimuth, C. Friedrich et al., "FLEUR (MaX-R7.2)", Zenodo, https://doi.org/10.5281/zenodo.13833162.
- [46] https://www.flapw.de/MaX-7.0/.
- [47] C. Friedrich, S. Blügel, and A. Schindlmayr, Efficient implementation of the *GW* approximation within the all-electron FLAPW method, Phys. Rev. B **81**, 125102 (2010).
- [48] C. Friedrich, M. C. T. D. Müller, J. Kirchmair, R. Sakuma, E. Sasioglu, M. Niesert, and S. Blügel, "Spex code (05.13.5)", Zenodo (2023), https://doi.org/10.5281/zenodo.14017762.
- [49] E. Şaşıoğlu, I. Galanakis, C. Friedrich, and S. Blügel, *Ab initio* calculation of the effective on-site Coulomb interaction parameters for half-metallic magnets, Phys. Rev. B **88**, 134402 (2013).
- [50] M. Tas, E. Şaşıoğlu, S. Blügel, I. Mertic, and I. Galanakis, *Ab initio* calculation of the Hubbard *U* and Hund exchange *J* in local moment magnets: The case of Mn-based full Heusler compounds, Phys. Rev. Mater. **6**, 114401 (2022).
- [51] G. Stollhoff, A. M. Oles, and V. Heine, Stoner exchange interaction in transition metals, Phys. Rev. B 41, 7028 (1990).
- [52] K. Koepernik and H. Eschrig, Full-potential nonorthogonal local-orbital minimum-basis band-structure scheme, Phys. Rev. B 59, 1743 (1999).
- [53] https://www.fplo.de/.
- [54] S. V. Halilov, H. Eschrig, A. Y. Perlov, and P. M. Oppeneer, Adiabatic spin dynamics from spin-density-functional theory: Application to Fe, Co, and Ni, Phys. Rev. B 58, 293 (1998).
- [55] R. A. Müller, A. Desilets-Benoit, N. Gauthier, L. Lapointe, A. D. Bianchi, T. Maris, R. Zahn, R. Beyer, E. Green, J. Wosnitza, Z. Yamani, and M. Kenzelmann, Magnetic structure of the antiferromagnetic half-Heusler compound NdBiPt, Phys. Rev. B 92, 184432 (2015).
- [56] J. Minar, Correlation effects in transition metals and their alloys studied using the fully self-consistent KKR-based LSDA + DMFT scheme, J. Phys.: Condens. Matter 23, 253201 (2011).

- [57] I. V. Solovyev, Combining DFT and many-body methods to understand correlated materials, J. Phys.: Condens. Matter 20, 293201 (2008).
- [58] K. Karlsson, F. Aryasetiawan, and O. Jepsen, Method for calculating the electronic structure of correlated materials from a truly first-principles LDA+U scheme, Phys. Rev. B 81, 245113 (2010).
- [59] F. Lechermann, A. Georges, A. Poteryaev, S. Biermann, M. Posternak, A. Yamasaki, and O. K. Andersen, Dynamical mean-field theory using Wannier functions: A flexible route to electronic structure calculations of strongly correlated materials, Phys. Rev. B 74, 125120 (2006).
- [60] E. H. Shourov, P. J. Strohbeen, D. Du, A. Sharan, F. C. de Lima, F. Rodolakis, J. L. McChesney, V. Yannello, A. Janotti, T. Birol, and J. K. Kawasaki, Electronic correlations in the semiconducting half-Heusler compound FeVSb, Phys. Rev. B 103, 045134 (2021).
- [61] G. Fischer, X. Zubizarreta, A. Marmodoro, M. Hoffmann, P. Buczek, N. Buczek, M. Däne, W. Hergert, E. Şaşıoğlu, I. Galanakis, and A. Ernst, Effect of correlation and disorder on the spin-wave spectra of Pd₂MnSn, Nd₂MnSn, and Cu₂MnAl Heusler alloys: A first-principles study, Phys. Rev. Mater. 4, 064405 (2020).
- [62] E. Şaşıoğlu, C. Friedrich, and S. Blügel, Effective Coulomb interaction in transition metals from constrained random-phase approximation, Phys. Rev. B 83, 121101(R) (2011).
- [63] S. Hong and J. I. Lee, Magnetism and the stoner exchange parameter of fcc palladium, J. Korean Phys. Soc. 52, 1099 (2008).
- [64] A. Lichtenstein, Magnetism: From Stoner to Hubbard, in Emergent Phenomena in Correlated Matter Lecture Notes of the Autumn School Correlated Electrons 2013, edited by E. Pavarini, E. Koch, and U. Schollwöck (Forshungzentrum Jülich, Jülich, Germany, 2013), pp. 151–185.
- [65] L. Sandratskii, Noncollinear magnetism in itinerant-electron systems: Theory and applications, Adv. Phys. 47, 91 (1998).
- [66] L. Nordström and D. J. Singh, Noncollinear intra-atomic magnetism, Phys. Rev. Lett. 76, 4420 (1996).
- [67] M. van Schilfgaarde and V. P. Antropov, First-principles exchange interactions in Fe, Ni, and Co, J. Appl. Phys. 85, 4827 (1999).
- [68] O. Grotheer, C. Ederer, and M. Fähnle, Fast *ab initio* methods for the calculation of adiabatic spin wave spectra in complex systems, Phys. Rev. B **63**, 100401(R) (2001).
- [69] E. Şaşıoğlu, L. M. Sandratskii, P. Bruno, and I. Galanakis, Exchange interactions and temperature dependence of magnetization in half-metallic Heusler alloys, Phys. Rev. B 72, 184415 (2005).
- [70] J. Rusz, L. Bergqvist, J. Kudrnovský, and I. Turek, Exchange interactions and Curie temperatures in Ni_{2-x}MnSb alloys: Firstprinciples study, Phys. Rev. B 73, 214412 (2006).
- [71] J. Kübler, G. H. Fecher, and C. Felser, Understanding the trend in the Curie temperatures of Co₂-based Heusler compounds: *Ab initio* calculations, Phys. Rev. B **76**, 024414 (2007).
- [72] S. Y. Savrasov, Linear response calculations of spin fluctuations, Phys. Rev. Lett. 81, 2570 (1998).
- [73] P. Buczek, A. Ernst, P. Bruno, and L. M. Sandratskii, Energies and lifetimes of magnons in complex ferromagnets: A firstprinciple study of Heusler alloys, Phys. Rev. Lett. 102, 247206 (2009).

- [74] E. Şaşıoğlu, A. Schindlmayr, C. Friedrich, F. Freimuth, and S. Blügel, Wannier-function approach to spin excitations in solids, Phys. Rev. B 81, 054434 (2010).
- [75] K. Karlsson and F. Aryasetiawan, Spin-wave excitation spectra of nickel and iron, Phys. Rev. B **62**, 3006 (2000).
- [76] C. Friedrich, E. Şaşıoğlu, M. Müller, A. Schindlmayr, and S. Blügel, Spin excitations in solids from many-body perturbation theory, in *First Principles Approaches to Spectroscopic*
- *Properties of Complex Materials*, edited by C. Di Valentin, S. Botti, and M. Cococcioni (Springer, Berlin, 2014), pp. 259–301.
- [77] A. T. Costa, Jr., R. B. Muniz, and D. L. Mills, Theory of spin waves in ultrathin ferromagnetic films: The case of Co on Cu (100), Phys. Rev. B **69**, 064413 (2004).
- [78] S. Lounis, A. T. Costa, R. B. Muniz, and D. L. Mills, Dynamical magnetic excitations of nanostructures from first principles, Phys. Rev. Lett. **105**, 187205 (2010).